Journal of Industrial and Engineering Chemistry 114 (2022) 323–330

Contents lists available at ScienceDirect

Journal of Industrial and Engineering Chemistry

journal homepage: www.elsevier.com/locate/jiec

The use of black mass in spent primary battery as an oxidative catalyst for removal of volatile organic compounds

Beom-Sik Kim [a], Sang-Chul Jung [b], Ho-Young Jung [c], Moonis Ali Khan [d], Byong-Hun Jeon [e], Sang Chai Kim [f,*]

[a] Hydrogen Research Center, Research Institute of Industrial Science and Technology, Pohang 37673, Republic of Korea
[b] Department of Environmental Engineering, Sunchon National University, Sunchon 57975, Republic of Korea
[c] Department of Environment and Energy Engineering, Chonnam National University, Gwangju 61186, Republic of Korea
[d] Chemistry Department, College of Science, King Saud University, Riyadh 11451, Saudi Arabia
[e] Department of Earth Resource and Environmental Engineering, Hanyang University, Seoul 04763, Republic of Korea
[f] Department of Environmental Education, Mokpo National University, Muan 58554, Republic of Korea

ARTICLE INFO

Article history:
Received 18 June 2022
Revised 6 July 2022
Accepted 13 July 2022
Available online 19 July 2022

Keywords:
Spent primary battery
Black mass
Complete oxidation
Volatile organic compounds
Catalyst

ABSTRACT

This work synthesized spent primary batteries (SPBs)-based (SB) catalyst from the black mass (BM) of the respective SPBs of R and D companies and tested it in the complete oxidation of volatile organic compounds (VOCs) to examine its effectiveness. In particular, benzene, toluene, and *o*-xylene (BTX) were chosen as representative VOCs. In addition, the physicochemical properties of the RSB and DSB catalysts prepared from the BMs in the SPBs of R and D companies, respectively, were characterized by ICP/OES, SEM/EDX, BET, XRD, TGA, O_2-TPO, H_2-TPR, and XPS analyses. Notably, the manganese-rich DSB catalyst had a higher activity compared to the RSB catalyst. Also, the dominant crystal phases of the RSB catalyst were of C, $ZnMn_2O_4$, Mn_3O_4, ZnO, and C_2K_2, and those of the DSB catalyst were of C and MnO_2. In particular, the manganese oxide species significantly influenced the catalytic activity. Furthermore, the lattice oxygen mobility of the catalyst contributed to the VOCs complete oxidation. In effect, the BTXs were completely oxidized at less than 380 and 360 °C over the RSB and DSB catalysts, respectively, at a gas hourly space velocity of 50,000 h^{-1}.

Introduction

Since primary batteries, such as manganese and alkaline batteries, are versatile, convenient, inexpensive, and essential for electronic devices, their consumption has been steadily increasing [1]. In particular, manganese and alkaline batteries are mainly used in electronic devices requiring small power [2]. Also, they are consumed and discarded in a short time, resulting in a lot of their waste. Moreover, these spent manganese and alkaline batteries contain heavy metals, including zinc, manganese, etc. And heavy metals can pose a serious threat to humans, animals, plants, and crops. Accordingly, SPBs must be safely disposed of as they may threaten the ecosystem [3–5]. In Korea, more than 15,000 tons of spent manganese and alkaline batteries were generated in 2020 [6]. Accordingly, it is strongly necessary to recycle the spent primary batteries, which accounts for a significant portion of the discarded batteries. Recently, the resourcization of SPBs has attracted increasing attention from an economic, environmental, and technological perspective [7,8]. Meanwhile, various research had focused on the recovery of valuable metals, such as manganese, zinc, etc., from SPBs [2,9,10].

Volatile organic compounds (VOCs) are some of the main pollutants with a boiling point of less than 260 °C under room temperature and atmospheric pressure conditions [11]. The main sources of VOCs, such as chemical plants, paint factories, printing shops, food processing, etc., are varied. Since the VOCs are highly toxic and volatile, they are regarded as important air pollutants [12,13]. Furthermore, the VOCs are also a causative agent of photochemical smog and have recently been recognized as substances causing ultrafine dust [14,15]. Therefore, the VOCs must be removed from their sources without being released into the atmosphere. Various technologies have been used for the VOCs removal, including condensation [16], adsorption [17], membrane separation [18], photocatalytic decomposition [19–21], plasma oxidation [22], ozone oxidation [23–26], biological decomposition [27], combustion [28], and catalytic oxidation [29]. Notably, catalytic oxidation is economical, compact, easy to operate, and efficient among these technologies. Also, transition metals as catalysts for the VOCs

* Corresponding author.
E-mail address: gikim@mokpo.ac.kr (S.C. Kim).

https://doi.org/10.1016/j.jiec.2022.07.022
1226-086X/

removal using catalytic oxidation are cheaper, are more resistant to poisons than precious metals, and have good performance [30–32].

The SPBs, such as spent manganese and alkaline batteries, contain transition metals (zinc, manganese, etc.). So, it is possible to use SPBs as a catalyst source for the VOCs removal [33–35]. Relatedly, manganese oxides recovered from spent zinc-carbon and alkaline batteries were used for the VOCs removal [8]. MnZnO and nanoscale manganese oxide catalysts for the VOCs oxidation were synthesized from spent zinc-carbon and alkaline batteries by using chemical precipitation [36,37]. Moreover, a multi-oxide catalyst based on manganese was synthesized from a spent lithium-ion battery through a biohydrometallurgical process and used for the VOCs complete oxidation [38]. Likewise, multi-metal oxides catalysts for oxygenated VOCs oxidation were prepared from spent lithium-ion batteries by different preparation methods, like combustion, co-precipitation, hydrothermal, etc. [39]. Recently, the Mn-Fe bimetallic oxide catalyst derived from spent alkaline battery was used for the oxidation of bisphenol A [40].

However, in terms of efficiency and economy, it may be preferable to use in bulk form without recovery and resynthesis of each component of the black mass (BM) inside spent primary batteries (SPBs). The BM composite material of the SPBs was used to catalyze the VOCs oxidation in this work. There are several types of SPBs with different components, and consequently the catalytic properties also are different. The effect of different catalytic properties of various types of SPBs on the removal of VOCs was not investigated at all. Accordingly, we compared the catalytic performances and properties of the BMs of the SPBs from different manufacturers (R and D companies) as VOCs oxidation catalysts. Also, benzene, toluene, and *o*-xylene (BTX) were chosen as representative VOCs for the test. Moreover, the physicochemical properties of the samples were characterized by Brunauer–Emmett–Teller (BET) isotherms, inductively coupled plasma/optical emission spectrometry (ICP/OES), X-ray diffraction (XRD), thermogravimetric analysis (TGA), oxygen-temperature-programmed oxidation (O_2-TPO), X-ray photoelectron spectroscopy (XPS), and hydrogen-temperature-programmed reduction (H_2-TPR).

Experiments

Synthesis of the catalysts

The BMs in the respective SPBs of R and D companies were used for the SB catalyst synthesis, as shown in Fig. 1. The separated black mass (4.0 g) from each battery was put into a flask containing 100 mL of deionized water. The resulting slurry was stirred with a shaker (KMC-8480SF, Vision Scientific), which worked at 150 rpm and at 30 °C for 5 h. The mixture was then filtered and washed three times with deionized water. Sulfuric acid (H_2SO_4 (95 %, Dae Jung) aqueous solution with a concentration of 0.1 N was used to treat the washed black masses. 3.0 g of each washed black mass was placed in the flask with 200 mL of the acidic solution. The mixture was treated in a shaker as described above to obtain a washed black mass. The samples treated with sulfuric acid aqueous solution were washed several times with deionized water for their pH to reach about 7, then dried at 80 °C for 24 h. The dried samples were finally calcined at 400 °C for 4 h in a furnace.

The synthesized catalysts were named RSB and DSB catalysts, respectively, where R and D denote the first letter of the company (that supplied the SPBs) name.

Characterization of the catalysts

Brunauer–Emmett–Teller (BET) measurements were performed using a Belsorp Mini II 2020 to determine the surface areas of the catalysts (N_2 adsorption at 25 °C). Before sorption analysis, all catalysts were degassed in a vacuum (5×10^{-3} mmHg) at 150 °C for 6 h. The elemental compositions of the catalysts were analyzed by inductively coupled plasma/optical emission spectroscopy (ICP/OES) using a Perkin Elmer Optima 8300. The samples were prepared for analysis using the microwave-assisted acid (aqua regia) digestion method. X-ray diffraction (XRD) was used to study the crystalline structures of the catalysts using a Phillips PW3123 diffractometer with Cu/Kα radiation of 0.154 nm. The catalysts were examined in the 2θ range of 20–90° at a scanning speed of 70° h^{-1}. A HITACHI S-4800 SEM (Hitachi, Japan) with an Oxford Link SATW ultrathin window EDX detector was used for SEM/EDX (scanning electron microscope/energy dispersive X-ray) analysis. Chemical components of the particle were determined from EDX data acquired in point mode at several spots within each particle. Thermo gravimetric analysis (TGA), using a PerkinElmer Pyris Diamond, was performed under a stream of air in the temperature range of 25–1000 °C (heating rate: 10 °C min^{-1}). Oxygen-temperature programmed oxidation (O_2-TPO) was carried out using a BEL-CAT setup. Prior to analysis, 0.4 g of the catalyst was pre-treated with 30 mL/min of He gas at 200 °C for 2 h. The temperature of the catalyst was then lowered to 50 °C. The catalyst sample was passed through the gas mixture (5 % O_2 and 95 % He) at a rate of 30 mL/min while the temperature was increased to 800 °C at a rate of 10 °C/min. The redox of the catalysts was examined with hydrogen-temperature programmed reduction (H_2-TPR) by the same experimental method as O_2-TPO. Pre-treated gas and reduction gas were used Ar and gas mixture of 5 % H_2 and 95 % Ar, respectively. X-ray photoelectron spectroscopy (XPS) (VG Scientific MultiLab 2000) was performed using non-monochromatic Mg Kα radiation with an energy of 1253.6 eV. The C1s peak (285.0 eV) obtained from XPS was used to calibrate the binding energy.

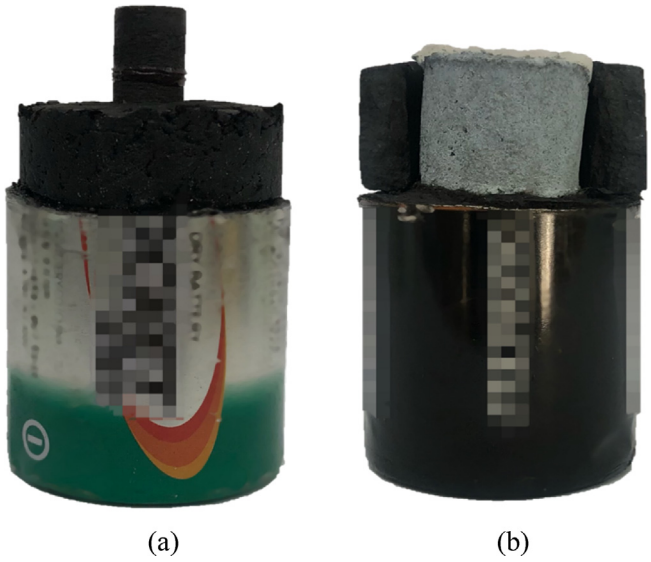

Fig. 1. Pictures of spent batteries for (a) RSB and (b) DSB catalysts.

BTX complete oxidation

The BTX complete oxidations over the RSB and DSB catalysts, respectively, were carried out in a catalytic oxidation test device [41]. A sample of the catalyst (60 mg) was placed in the center of the reactor. It was supported by quartz wool. Commercial BTXs (Fisher) were used for the experiment. An air stream was passed through each benzene, toluene or *o*-xylene saturator. Mass flow

controllers (UFC-8100) were used to accurately and stably adjust the gas flow rates. Each reactant concentration was maintained at 1000 ppm, which was adjusted using a saturator temperature. Reactant flow was indicated using a gas hourly space velocity of 50,000 h^{-1}. All tubes were kept at 110 °C to prevent adsorption and condensation of the reactant and product in the lines. Experimental data were taken after confirming that all reaction conditions had reached a steady state (i.e. when the temperature and reactant flow became constant). Inlet and outlet concentrations were measured using a gas chromatograph (GC-14A, Shimadzu) with a thermal conductivity detector (TCD). The column packing consisted of 5 % bentone-34 and 5 % DNP/shimalite (3 mm ø × 3 m, 60–80 mesh) for BTXs separations, while a Porapak Q (3 mm ø × 3 m, 50–80 mesh) was used to measure the concentration of CO_2. A GC with a mass spectrometry (GC/MS-QP5050, Shimadzu) was also used to quantitatively and qualitatively analyze the reactants and products. Only CO_2 and H_2O were produced in all experimental conditions without any other products. The hydrocarbon conversions were calculated based on the consumption of each reactant.

Results and discussion

Characterization of the RSB and DSB catalysts

The morphologies and surface components of the RSB and DSB catalysts were examined by SEM/EDX. The SEM images and the corresponding EDX spectra of the RSB and DSB catalysts are shown in Fig. 2. The EDX spectra and Table 1 reveal that the surface elements of the RSB catalyst were composed of zinc, manganese, iron, carbon, oxygen, aluminium, silicon, sodium, potassium, and chlorine, while those of the DSB catalyst consisted of zinc, manganese, carbon, oxygen, and potassium. In addition, the main transition metal components of the RSB catalyst were zinc, manganese, iron, and while that of the DSB catalyst was manganese. In particular, the surface manganese concentration of the DSB catalyst was approximately twice higher than that of the RSB catalyst. Furthermore, the ICP/OES measurement results of the RSB and DSB catalysts are summarized in Table 2. This also reveals that the manganese concentration of the DSB catalyst was about twice higher than that of the RSB catalyst, in accordance with the EDX spectra. Meanwhile, aluminium and sodium, which did not appear in the EDX spectra of the DSB catalyst, appeared in the ICP/OES measurement results of the catalyst, suggesting that aluminium and sodium existed inside the catalyst and not on its surface. Also, it seemed that silicon was removed during the respective pretreatment of the RSB and DSB catalyst samples for the ICP/OES measurement. In addition, both the ICP/OES measurement and SEM/EDX examination showed that the amount of manganese in the DSB catalyst was about twice higher than that of the RSB catalyst.

The BET surface areas, mean pore diameters, and total pore volumes of the catalysts are summarized in Table 3. Notably, the BET surface areas of the RSB and DSB catalysts were 45.1 and 31.1 m^2/g, respectively. In addition, their total pore volumes and mean pore diameters and were 0.18 cm^3/g and 16.0 nm, and 0.11 cm^3/g and 15.1 nm, respectively.

Fig. 3 shows the 20,000-fold magnified SEM images of the morphologies of the RSB and DSB catalysts. These magnified SEM images of the RSB catalyst show that the catalyst surface looked like swollen blossoms (Fig. 3(a)). On the other hand, the DSB catalyst surface seemed to have molten or spread small particles (Fig. 3 (b)). These morphologies also showed that the RSB catalyst surface area was larger than that of the DSB catalyst, consistent with the BET surface areas given in Table 3.

Fig. 4 shows the XRD patterns of the RSB and DSB catalysts. Notably, the main crystal phases of the RSB catalyst were of $ZnMn_2O_4$, ZnO, Mn_3O_4, C, and C_2K_2, and those of the DSB catalyst were only the C and MnO_2 crystal phases.

Fig. 5 shows the carbon weights of the RSB and DSB catalysts measured by the TGA in a dynamic oxygen atmosphere. The TG curve of the RSB catalyst shows that the catalyst weight loss at

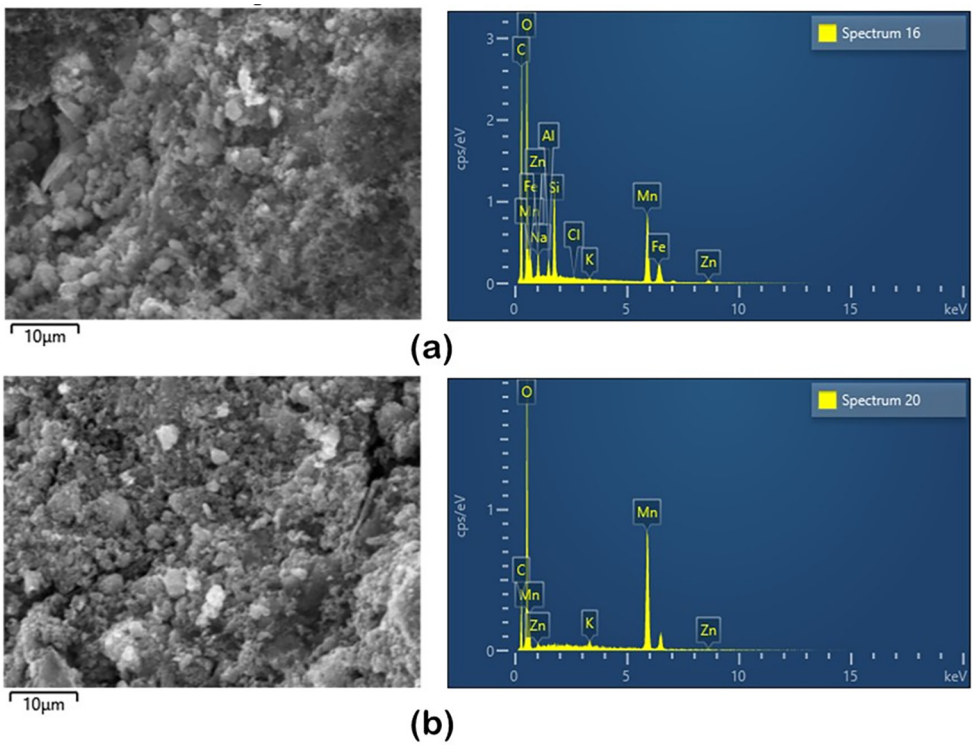

Fig. 2. SEM images and corresponding EDX spectra of (a) RSB and (b) DSB catalysts.

Table 1
Components of RSB and DSB catalyst measured by SEM/EDX.

Elements (wt. %)	Zn	Mn	Fe	C	O	Al	Si	Na	K	Cl
RSB	7.0	24.1	8.2	24.6	28.8	1.5	5.0	0.4	5.2	0.1
DSB	0.4	50.4	–	19.0	29.7	–	–	–	0.5	–

Table 2
Elements of RSB and DSB catalysts measured by ICP/OES.

Elements (wt. %)	Zn	Mn	Fe	Al	Si	Na	K
RSB	15.10	32.80	8.09	1.16	N.D.	0.03	0.27
DSB	0.67	59.00	N.D.	0.79	N.D.	0.19	0.67

N.D.: Not Determined.

Table 3
Textual properties of the RSB and DSB catalysts.

Catalyst	BET surface area (m^2/g)	Total pore volume (cm^3 /g)	Mean pore diameter (nm)
RSB	45.1	0.18	16.0
DSB	31.1	0.11	15.1

temperatures up to 150 °C was around 2.3 wt. %. This weight loss was due to the desorption of impurities and water on the catalyst surface. However, this TG curve shows inflection points at 485 and 615 °C and a considerable weight loss at these points that continued up to 750 °C, which was attributed to carbon oxidation [42]. On the other hand, the weight loss of the DSB catalyst at temperatures up to 150 °C was around 0.72 wt. %. Furthermore, the weight loss rate of the RSB catalyst was greater than that of the DSB catalyst, indicating more impurities and water on the surface of the RSB catalyst than those of the DSB catalyst, respectively. Meanwhile, the inflection points in the TG curve of the DSB catalyst were at 465 and 565 °C.

Fig. 6 shows the TPO patterns of the RSB and DSB catalysts. The TPO pattern of the RSB catalyst had two peaks at 559 and 615 °C due to the two carbon species of the catalyst [43]. In the same way, the TPO pattern of the DSB catalyst had two peaks at 532 and 584 °C. Accordingly, the TPO patterns were in good agreement with the TGA measurements. In other words, TPO patterns of the RSB and DSB catalysts showed two peaks each, corresponding to the two inflection points in each of their TGA curves.

Since the redox properties of a catalyst often play an important role in the catalytic activity, H_2-TPR experiments of the RSB and DSB catalysts were performed to study the redox properties of the catalysts. Fig. 7 shows the TPR patterns of the RSB and DSB catalysts. The calculated values of hydrogen consumption, starting temperature of the TPR peak (STP), and temperature of the TPR peak (TTP) of the RSB and DSB catalysts, respectively, are listed in Table 4. Notably, two reduction peaks due to the reduction of metal oxides species were observed in the TPR pattern of both RSB and DSB catalysts. In addition, Fig. 7 shows that the STP and TTPs of the two reduction peaks in the TPR pattern of the RSB catalyst were 260, 347, and 492 °C, whereas they were 220, 322, and 410 °C in the TPR pattern of the DSB catalyst, respectively. In addition, the TPR pattern of the RSB catalyst shows that the amount of hydrogen consumed in the first and second peaks were 1.19 and

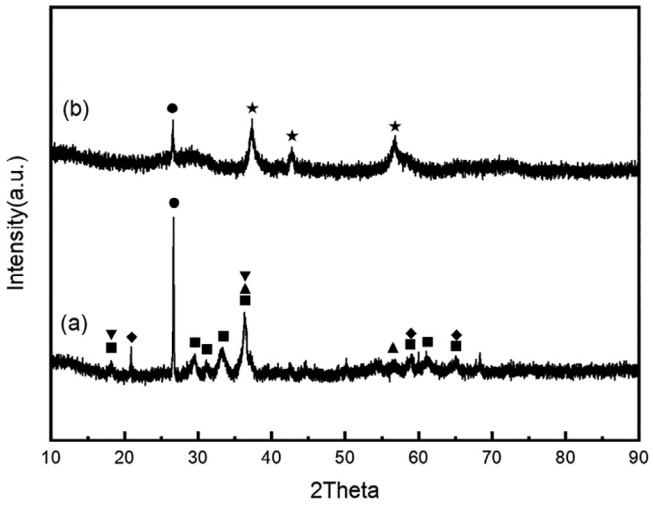

Fig. 4. XRD patterns of (a) RSB and (b) DSB catalysts.

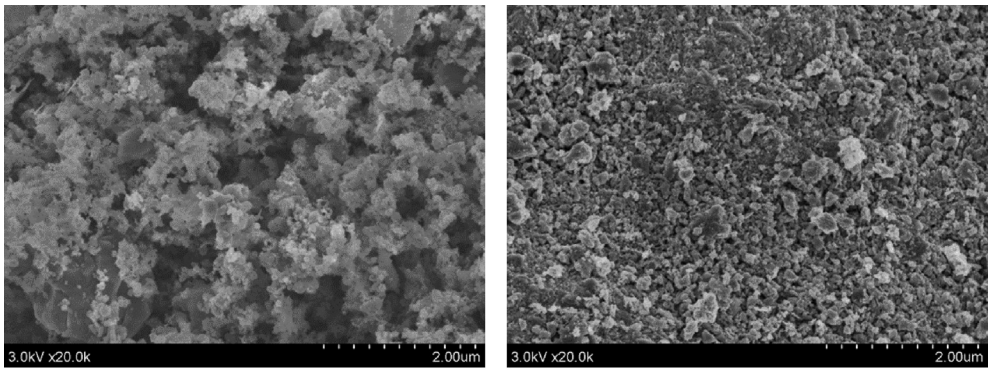

Fig. 3. SEM images of (a) RSB and (b) DSB catalysts.

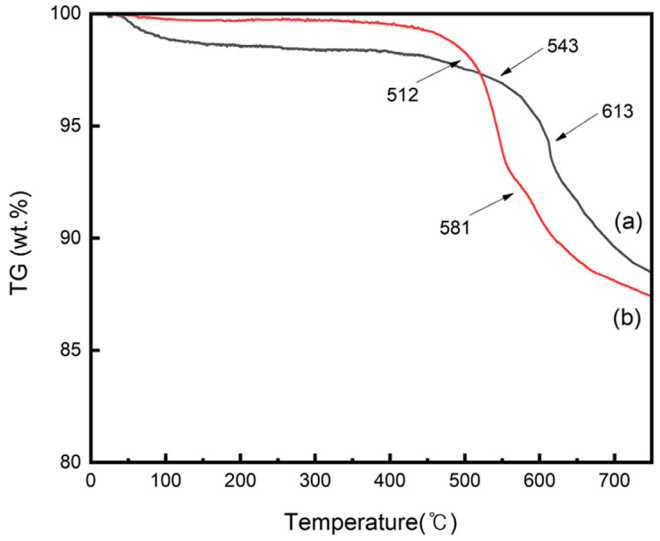

Fig. 5. TGA patterns of (a) RSB and (b) DSB catalysts.

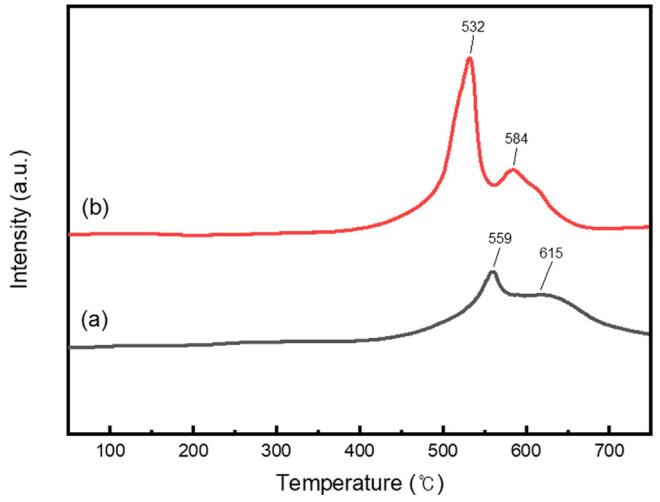

Fig. 6. TPO patterns of (a) RSB and (b) DSB catalysts.

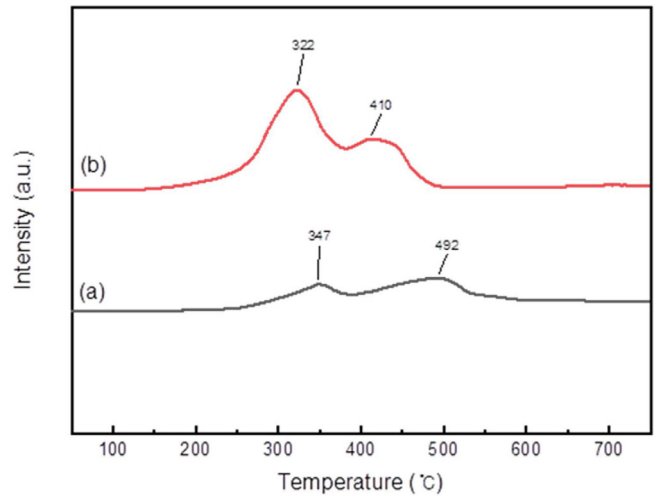

Fig. 7. TPR patterns of (a) RSB and (b) DSB catalysts.

Table 4
Hydrogen consumption, Starting temperature of TPR peak, and temperature of TPR peak of the RSB and DSB catalysts.

Catalyst	Hydrogen consumption (mmol/g)	Starting temperature of TPR peak (°C)	Temperature of TPR peak (°C)
RSB	1.19[a], 1.84[b]	260	347[a], 492[b]
DSB	4.66[a], 1.97[b]	220	322[a], 410[b]

[a] 1st peak.
[b] 2nd peak.

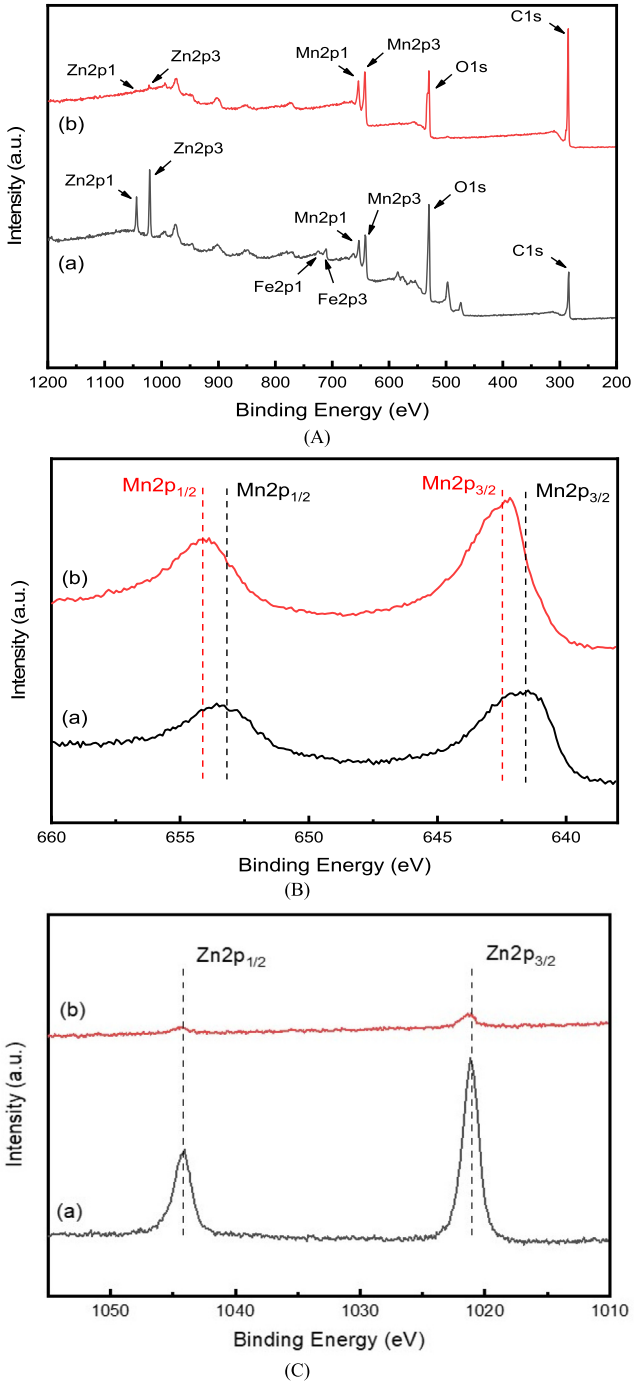

Fig. 8. XPS spectra of the survey scan (A), the Mn 2p region (B), and the Zn 2p region (C) of samples. (a) RSB and (b) DSB catalysts.

1.84 mmol/g, respectively. On the other hand, the TPR pattern of the DSB catalyst shows that the amount of hydrogen consumed in the first and second peaks were 4.66 and 1.97 mmol/g, respectively. Additionally, the compositions and surface electronic states of the RSB and DSB catalysts were characterized by XPS.

shows the survey scan spectra and XPS spectra evolutions of the RSB and DSB catalysts. Notably, the survey scan spectra (Fig. 8(A)) confirm manganese, zinc, iron, carbon, and oxygen in the RSB catalyst and manganese, zinc, carbon, and oxygen in the DSB catalyst. Also, Fig. 8(B) and (C) shows the manganese and zinc XPS spectra evolutions, respectively. The binding energies (BEs) of Mn 2p and Zn 2p are listed in Table 5. In particular, the BEs of Mn $2P_{1/2}$ and Mn $2p_{3/2}$ of the RSB catalyst were 653.18 and 641.57 eV, and those of the DSB catalyst were 654.12 and 642.48 eV, respectively. These BEs indicated that the BE of Mn 2p of the RSB catalyst corresponded to Mn_3O_4, whereas that of the DSB catalyst corresponded to MnO_2 [33]. Meanwhile, the ICP/OES measurement and EDX spectra showed that the zinc concentration in the DSB catalyst was much lower than that in the RSB catalyst. Likewise, the zinc XPS spectrum (Fig. 8(C)) showed that the zinc intensity in the zinc XPS spectrum of the RSB catalyst was much higher than that of the DSB catalyst. On the other hand, the BEs of Zn $2p_{1/2}$ and Zn $2p_{3/2}$ of the RSB catalyst were 1044.09 and 1021.00 eV, and those of the DSB catalyst were 1044.82 and 1021.02 eV, respectively. In particular, the BE difference between Zn $2p_{1/2}$ and Zn $2p_{3/2}$ of about 23.8~23.1 eV could be classified as ZnO (Zn^{2+}) [44,45]. Accordingly, the XPS spectra were in good agreement with the XRD profiles. No observed ZnO crystal phase in the XRD profiles indicated that it did not develop due to its low concentration.

Relationship between activities and characteristics of the RSB and DSB catalysts.

Fig. 9 shows the BTX conversions over the RSB and DSB catalysts, respectively, at different temperatures. T_{50} and T_{90} (temperature representing 50 % and 90 % conversion, respectively) of the BTX over the RSB and DSB catalysts, respectively, are listed in Table 6.

Notably, the T_{50} and T_{90} of benzene over the RSB catalyst were 309 and 352 °C, respectively. In contrast, these T_{50} and T_{90} over the DSB catalyst were 279 and 337 °C, respectively. The T_{50} and T_{90} of toluene and *o*-xylene over the RSB catalyst were 317 and 335 °C, and 327 and 339 °C, whereas these T_{50} and T_{90} over the DSB catalyst were 272 and 300 °C, and 253 and 276 °C, respectively. Generally, an aromatic compound having methyl derivatives with low ionization potential was easily oxidized [46]. In addition, the ionization potentials of the methyl derivative contained in *o*-xylene, toluene, and benzene are 8.56, 8.82, and 9.24 eV, respectively. Accordingly, the BTXs conversions reported above confirmed that the smaller the ionization potential of the methyl derivative, the easier the compound was oxidized over the RSB and DSB catalysts, respectively.

Generally, a catalyst with a large BET surface area is known to have good activity. Still, the activity of the DSB catalyst with a small surface area, mean pore diameter, and total pore volume was superior to that of the RSB catalyst. Therefore, the textual properties of a catalyst do not significantly affect the catalytic activity for the BTX oxidation. The manganese concentration of the DSB catalyst was also about twice higher than that of the RSB catalyst, indicating that the manganese-rich DSB catalyst had superior activity compared to the RSB catalyst. In addition, the main crystal phases of the RSB catalyst were of $ZnMn_2O_4$, ZnO, Mn_3O_4, C, and C_2K_2, whereas those of the DSB catalyst were only of C and MnO_2. Accordingly, the MnO_2 appeared to have acted as a better active site than other manganese oxide species, such Mn_3O_4 and $ZnMn_2O_4$.

Table 5
BEs (eV) of the Mn 2p and Zn 2p for the RSB and DSB catalysts.

Name	Mn $2p_{1/2}$	Mn $2p_{3/2}$	Zn $2p_{1/2}$	Zn $2p_{3/2}$
RSB	653.18	641.57	1044.09	1021.00
DSB	654.12	642.48	1044.82	1021.02

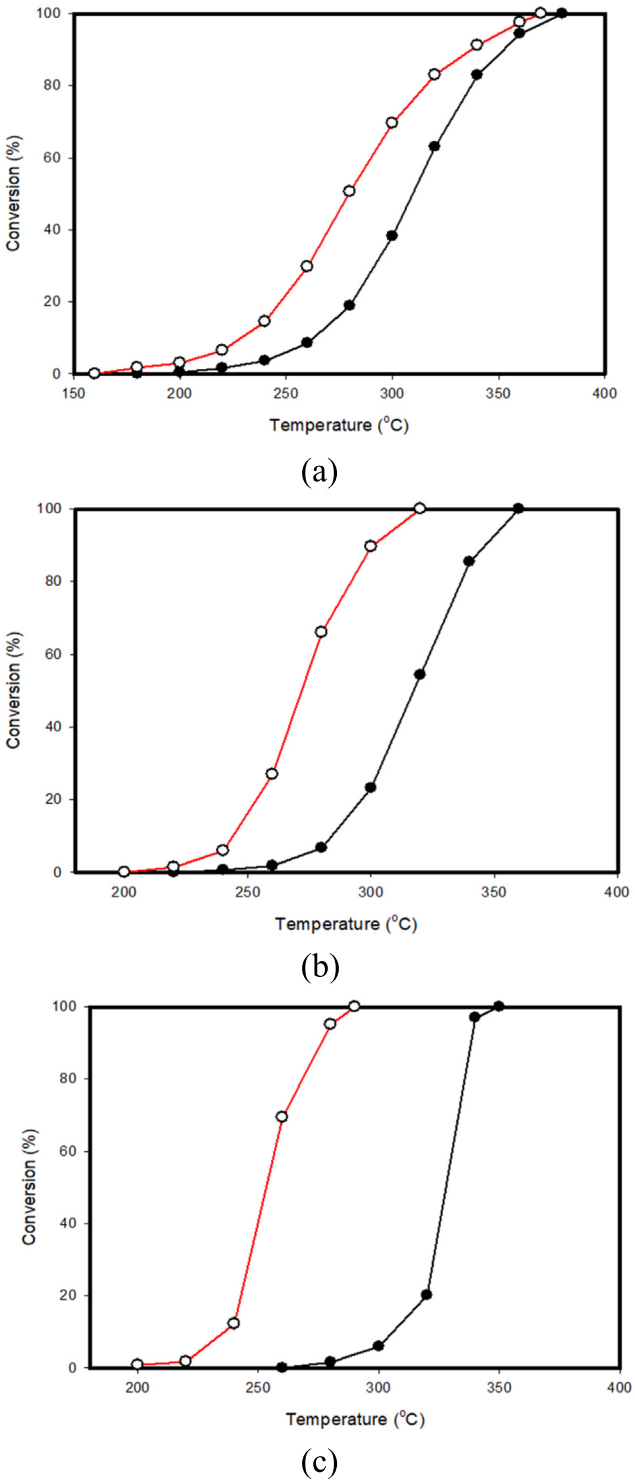

Fig. 9. (a) Benzene, (b) toluene), and (c) *o*-xylene conversions according to reaction temperature. (Reactant concentration = 1000 ppm, Gas Hourly Space Velocity = 50,000 h^{-1}).

Table 6
T_{50} and T_{90} of BTX over the RSB and DSB catalysts.

Catalyst	Benzene		Toluene		*o*-Xylene	
	T_{50}	T_{90}	T_{50}	T_{90}	T_{50}	T_{90}
RSB	309	352	317	345	327	339
DSB	279	337	272	300	253	276

Meanwhile, the TPR patterns indicated that the reduction temperature of lattice oxygen in the DSB catalyst was lower than that in the RSB catalyst. Therefore, the lattice oxygen of the DSB catalyst, which was more mobile than that of the RSB catalyst, favorably affected the oxidation of the carbon species of the catalyst, so that the TPO peak of the DSB catalyst was observed at a temperature lower than that of the TPO peak of the RSB catalyst. In other words, the lower the temperature of TPR peak, the more readily the catalyst's lattice oxygen can move, and this easily moving lattice oxygen contributes to the complete oxidation of VOCs [47–49]. These results indicate that the VOCs were adsorbed on the metal of the catalyst and the active lattice oxygen can easily oxidize the VOCs with the methyl derivatives with the low ionization potential.

Conclusion

The black mass (BM) of spent primary batteries (SPBs) was tested for its effectiveness as a VOCs oxidation catalyst. The DSB catalyst with a high manganese concentration had superior activity compared to the RSB catalyst with a low manganese concentration. The catalyst textual properties, particularly the surface area, mean pore diameter, and total pore volume, had an insignificant effect on the catalytic activity. In addition, the main crystal phases of the RSB catalyst were of $ZnMn_2O_4$, ZnO, Mn_3O_4, C, and C_2K_2, whereas those of the DSB catalyst were only of C and MnO_2. The MnO_2 seemed to have acted as a better active site than other manganese oxide species, such Mn_3O_4 and $ZnMn_2O_4$. Further, the DSB catalyst with carbon species oxidized at low temperatures showed the higher catalytic activity than the RSB catalyst with carbon species oxidized at high temperatures. The reduction temperature of lattice oxygen in the DSB catalyst was lower than that in the RSB catalyst. Hence, the lattice oxygen of the DSB catalyst, which was more mobile than that of the RSB catalyst, significantly affected the facile oxidation of the carbon species of the catalyst. Consequently, this readily mobile lattice oxygen contributed to the VOCs complete oxidation. Notably, the complete oxidation temperatures of BTXs over the RSB and DSB catalysts were 380, 360, and 350 °C, and 360, 320, and 290 °C, respectively, at a gas hourly space velocity of 50,000 h^{-1}. Overall, the spent primary battery-based (SB) catalyst can be promising for the VOCs complete oxidation.

Declaration of Competing Interest

The authors declare that they have no known competing financial interests or personal relationships that could have appeared to influence the work reported in this paper.

Acknowledgements

This research was supported by the Basic Science Research Program of the National Research Foundation of Korea (NRF) funded by the Ministry of Science and ICT (2022R1A2C100639111). Moonis Ali Khan acknowledges the financial support through Researchers Supporting Project number (RSP-2021/ 345), King Saud University, Riyadh, Saudi Arabia.

References

[1] C.C.B.M. De Souza, D.C. De Oliveira, J.A.S. Tenorio, J. Power Sources. 103 (1) (2001) 120.
[2] E. Sayilgan, T. Kukrer, G. Civelekoglu, F. Ferella, A. Akcil, F. Veglio, et al., Hydrometallurgy. 97 (2009) 158.
[3] W.-Q. Wang, H.-H. Chen, W.-J. Zhao, K.-M. Fang, H.-J. Sun, F.-Y. Zhu, Chemosphere 287 (2022) 132120.
[4] W. Wu, P. Bromberg, J.M. Samet, Free Radical Biol. Med. 65 (2013) 57.
[5] B. Chen, J. Luo, M. Hendryz, Environ. Res. 142 (2015) 96.
[6] KBRA (Korea Battery Recycling Association) Report, 2020.
[7] C.J. Rydh, M. Karlstrom, Resour. Conserv. Recycl. 34 (2002) 289.
[8] M.V. Gallegos, L.R. Falco, M.A. Peluso, J.E. Sambeth, H.J. Thomas, Waste Manage. 33 (2013) 1483.
[9] Z. Yang, W. Uhrynowski, G. Jakusz, J. Retka, J. Karczewska-Golec, K. Debiec-Andrzejewska, et al., Hydrometallurgy 191 (2020) 105223.
[10] X. Hu, A. Robeles, T. Vikström, P. Väänänen, M.Z.G. Ye, J. Hazard Mater. 411 (2021) 124928.
[11] J.E. Lee, Y.S. Ok, D.C.W. Tsang, J. Song, S.C. Jung, Y.K. Park, Sci. Total Environ. 719 (2020) 137405.
[12] U. Pöschl, M. Shiraiwa, Chem. Rev. 115 (2015) 4440.
[13] C. He, J. Cheng, X. Zhang, M. Douthwaite, Z. Hao, Chem. Rev. 119 (2019) 4471.
[14] Z. He, Y.J. Kim, K.O. Ogunjobi, J.E. Kim, S.Y. Ryu, Atoms. Environ. 38 (2004) 1795.
[15] M. Hallquist, J. Munthe, M. Hu, T. Wang, C.K. Chan, J. Gao, J. Boman, S. Guo, A.M. Hallquist, J. Mellqvist, J. Moldanova, R.K. Pathak, J.B.C. Pettersson, H. Pleijel, D. Simpson, M. Thynell, 3(4) (2016) 401.
[16] X. Li, J. Ma, X. Ling, Cryogenics 107 (2020) 103060.
[17] X. Shen, X. Du, D. Yang, J. Ran, Z. Yang, Y. Chen, J. Environ. Chem. Eng. 9 (2021) 106729.
[18] C. Zhang, X. Gao, J. Qin, Q. Guo, H. Zhou, W. Jin, J. Hazard. Mater. 402 (2021) 123817.
[19] M. Hussain, N. Russo, G. Saracco, Chem. Eng. J. 166 (2011) 138.
[20] N. Abbas, M. Hussain, N. Russo, G. Saracco, Chem. Eng. J. 175 (2011) 330.
[21] M. Hussain, P. Akhter, J. Iqbal, Z. Ali, W. Yang, N. Shehzad, et al., J. Environ. Chem. Eng. 5 (2017) 3100.
[22] X. Tang, F. Feng, L. Ye, X. Zhang, Y. Huang, Z. Liu, et al., Catal. Today 211 (2013) 39.
[23] J. Kim, E.E. Kwon, J.E. Lee, S.H. Jang, J.K. Jeon, J. Song, et al., J. Hazard. Mater. 403 (2021) 123934.
[24] J. Kim, J.E. Lee, H.W. Lee, J.K. Jeon, J. Song, S.C. Jung, et al., J. Hazard. Mater. 397 (2020) 122577.
[25] H.W. Ryu, M.Y. Song, J.S. Park, J.M. Kim, S.C. Jung, J. Song, et al., Environ. Res. 172 (2019) 649.
[26] K.H.P. Reddy, B.S. Kim, S.S. Lam, S.C. Jung, J. Song, Y.K. Park, Environ. Res. 195 (2021) 110876.
[27] P. Saingam, Z. Baig, Y. Xu, J. Xi, J. Environ. Sci. 69 (2018) 133.
[28] M. Tomatis, M.T. Moreira, H. Xu, W. Deng, J. He, A.M. Parvez, J. Cleaner Prod. 233 (2019) 808.
[29] V. Brummer, S.Y. Teng, D. Jecha, P. Skryja, V. Vavrcikova, P. Stehlik, J. Cleaner Prod. 361 (2022) 132112.
[30] Y. Shi, X. Guo, Z. Shi, R. Zhou, J. Rare Earth 40 (5) (2022) 745.
[31] C.H. Wang, S.S. Lin, C.L. Chen, H.S. Weng, Chemosphere 64 (2006) 503.
[32] S. Mo, S. Li, W. Li, J. Li, J. Chen, Y. Chen, J. Mater. Chem. A 4 (2016) 8113.
[33] M. Piumetti, D. Fino, N. Russo, Appl. Catal. B: Environ. 163 (2015) 277.
[34] S.C. Kim, W.G. Shim, Appl. Catal. B: Environ. 98 (2010) 180.
[35] F.G. Durán, B.P. Barbero, L.E. Cadús, C. Rojas, M.A. Centeno, J.A. Odriozola, Appl. Catal. B: Environ. 92 (2009) 194.
[36] S. Hoseini, N. Rahemi, S. Allahyari, M. Tashihi, J. Cleaner Prod. 232 (2019) 1134.
[37] M.V. Gallegos, M.A. Peluso, E. Finocchio, H.J. Thomas, G. Busca, J.E. Sambeth, Chem. Eng. J. 313 (2017) 1099.
[38] M. Guo, K. Li, L. Liu, H. Zhang, W. Guo, X. Hu, et al., J. Hazard. Mater. 380 (2019) 120905.
[39] M. Guo, X. Wang, L. Liu, X. Min, X. Hu, W. Guo, N. Zhu, J. Jia, T. Sun, K. Li, Environ. Res. 193 (2021) 110563.
[40] Y. Ma, D. Wang, Y. Xu, H. Lin, H. Zhang, J. Hazard. Mater. 436 (2022) 129172.
[41] S.C. Kim, S.W. Nahm, Y.K. Park, J. Hazard. Mater. 300 (2015) 104.
[42] S.A. Charef, A.M. Affoune, A. Caballero, M. Cruz-Yusta, J. Morales, Waste Manage. 68 (2017) 518.
[43] J.E. Herrera, D.E. Resasco, Chem. Phys. Lett. 376 (2003) 302.
[44] Z.H. Zhu, Z.B. Wang, Z.E. Yan, R.Q. Zhou, Z.P. Wang, C.N. Chen, Ceram. Int. 44 (2018) 10163.

[45] B. Chen, X. Yang, X. Zeng, Z. Huang, J. Xiao, J. Wang, et al., Chem. Eng. J. 397 (2020) 12424.
[46] L. Becker, H. Förster, Appl. Catal. B: Environ. 17 (1–2) (1998) 43.
[47] S.M. Saqer, D.L. Kondarides, X.E. Verykios, Appl. Catal. B: Environ. 103 (2011) 275.
[48] W.G. Shim, J.W. Nah, H.Y. Jung, Y.K. Park, S.C. Jung, S.C. Kim, J. Ind. Eng. Chem. 60 (2018) 259.
[49] E. Yu, J. Li, J. Chen, J. Chen, Z. Hong, H. Jia, J. Hazard. Mater. 388 (2020) 121800.